



1 **External and Internal CCN Mixtures: Controlled Laboratory Studies of Varying Mixing**
2 **States.**

3 Diep Vu^{1,2,§}, Shaokai Gao^{1,♦}, Tyler Berte^{1,2}, Mary Kacarab^{1,2,♠}, Qi Yao⁴, Kambiz Vafai³ and Akua Asa-Awuku^{1,2,4,*}

4

5 1.*Department of Chemical and Environmental Engineering, Bourns College of Engineering, University of
6 California, Riverside, CA 92521, USA

7 2.*Bourns College of Engineering, Center for Environmental Research and Technology (CE-CERT), Riverside, CA
8 92507, USA

9 3. Department of Mechanical Engineering, Bourns College of Engineering, University of California, Riverside, CA
10 92521, USA

11 4.*Department of Chemical and Biomolecular Engineering, A. James Clark School of Engineering, University of
12 Maryland, College Park, MD 20742.

13

14 §. Currently at Ford Motor Company, Research & Innovation Center Dearborn, MI 48124, USA

15 ♦. Currently at Phillip 66 Research Center, Research and Development, Bartlesville, OK 74004, USA

16 ♠. Currently at Georgia Institute of Technology, Atlanta, GA 30309, USA

17

18 *Correspondence to: A. Asa-Awuku (asaawuku@umd.edu)

19

20 **Abstract**

21

22 Particle mixing states modify CCN activity. A method of cloud condensation nuclei (CCN) data analysis for
23 multicomponent mixtures of varying mixing states and its relationship to activation curves consisting of one or more
24 activation points is presented. Simplified two component systems of varying solubility were generated under internal,
25 external, and transitional mixing conditions. κ -Köhler theory predictions were calculated for different organic and
26 inorganic mixtures and compared to experimentally derived kappa values and respective mixing states. This work



27 employs novel experimental methods to provide information on the shifts in CCN activation data due to external to
28 internal particle mixing from controlled laboratory sources. Results show that activation curves consisting of single
29 and double activation points are consistent with internal and external mixtures, respectively. In addition, the height of
30 the plateau at the activation points are reflective of the externally mixed concentration in the mixture. The presence of
31 a plateau indicates that CCN activation curves consisting of multiple inflection points are externally mixed aerosols
32 of varying water-uptake properties. The plateau disappears when mixing is promoted in the flow tube. At the end of
33 the flow tube experiment, the aerosol are internally mixed and the CCN activated fraction data can be fit with a single
34 sigmoidal curve. The technique to mimic external to internally mixed aerosol is applied to non-hygroscopic
35 carbonaceous aerosol with organic and inorganic components. To our knowledge, this work is the first to show
36 controlled CCN activation of mixed non-hygroscopic black carbon with hygroscopic material as the aerosol population
37 transitions from external to internally mixed. Results confirm that CCN activation analysis methods are robust and
38 may be used to infer the mixing state of complex aerosol compositions of unknown origin.

39 1. Introduction

40 Atmospheric cloud condensation nuclei (CCN) are comprised of complex mixtures of organic and inorganic
41 compounds. The chemical and physical diversity present in these complex mixtures can significantly complicate the
42 quantification of aerosol-cloud interactions, thereby making it difficult to predict CCN activity. However,
43 knowledge of the mixing state and the chemical composition can greatly improve CCN predictions and has been the
44 focus of several studies (Abbatt et al., 2005; Bilde et al., 2004; Henning et al., 2005; Liu et al., 2013; Padró et al.,
45 2012; Svenningsson et al., 2006).

46 It is well accepted that the water content and the point of activation is dependent on more factors than just the
47 supersaturation and dry diameter for CCN active aerosols (Dusek et al., 2006; Petters and Kreidenweis, 2007). The
48 droplet growth and activation of slightly soluble inorganics can be modified when internally mixed with inorganic
49 salts that readily deliquesce (Cruz et al., 1998; Padró et al., 2002; Svenningsson et al., 2006). Although inorganic salts
50 are well characterized, the quantification of CCN activity is complicated when they are internally mixed with a
51 complex organic. Consequently, simple mixing rules may no longer be appropriate. It has been observed that mixed
52 aerosols can activate at lower supersaturations than their bulk constituents and organic compounds that may not



53 traditionally be considered as water soluble may aid in the formation of a cloud droplet by acting as a surfactant,
54 depressing surface tension, or simply by contributing mass (Cruz et al., 1998; Padró et al., 2007; Svenningsson et al.,
55 2006). In addition, when there is a sufficiently large enough fraction of salt, the slightly soluble core can dissolve
56 before activation, thus lowering the required supersaturation (Sullivan et al., 2009). Thus, the mixing state and extent
57 of mixing can substantially influence CCN activity.

58 To help minimize the complexity in characterizing aerosol hygroscopic and CCN activation properties, CCN data
59 analysis has been simplified by assuming that the aerosols share a similar or uniform hygroscopicity over a particle
60 size distribution, the CCN mobility diameter data sets consist of few doubly charged aerosols and all CCN active
61 aerosols readily dissolve at activation. As a result, a singular sigmoidal fit is commonly applied over the entire CCN
62 sample. However, this method of analysis may not be fully representative of the heterogeneous mixing state
63 occasionally present in the aerosol sample.

64 Previous studies have addressed aerosols with singular or internally mixed binary chemical species (Bilde et al.,
65 2004; Broekhuizen et al., 2004; Petters and Kreidenweis, 2007; Shulman et al., 1996; Sullivan et al., 2009). However,
66 ambient measurements indicate complex aerosol populations consisting of both external and internal mixtures (Ervens
67 et al., 2007; Lance et al., 2012; Padró et al., 2012). By accounting for the mixing states and extent of mixing in field
68 data sets, CCN concentration predictions can be greatly improved (Padró et al., 2012; Wex et al., 2010). However,
69 dynamic changes in particle mixing states and subsequent treatment of CCN measurement and analysis have not been
70 readily observed and studied in depth.

71 In this work, we seek to improve the experimental CCN activation analysis techniques of complex mixtures by
72 investigating the influence of mixing state on activation curves with known aerosol composition. Theoretical
73 postulations have been explored and applied to ambient data sets (e.g., but not limited to, Bhattu et al., 2016; Padró et
74 al., 2012) but never before has a systematic laboratory experiment controlled and modified the extent of particle
75 heterogeneity for CCN activation. To understand the impact of mixing state on CCN activation, simplified two
76 component mixtures of known compounds with varying hygroscopicities are created under internal, external, and in-
77 between (transition) mixing conditions. In addition, black carbon (BC) and BC mixing state data is presented. BC is
78 renown for its direct radiative effects yet little is known experimentally about the contributions of BC to aerosol-cloud
79 interactions at varied mixing states. Here, the hygroscopic properties of black carbon mixed with atmospherically
80 relevant constituents of varying hygroscopicity are investigated. This work provides evidence on the stark differences



81 between inorganic, slightly soluble, and insoluble externally and internally mixed compositions for the uptake of
82 water, and subsequent CCN activity.

83

84 **2. Experimental Methods**

85 **2.1 Aerosol Composition and Sources**

86

87 The CCN activity of two component aerosol mixtures under internal, external, and combinations of mixing states
88 are explored in this study. The components include very hygroscopic (inorganics), hygroscopic (organic acids), and
89 non-hygroscopic (Black Carbon, BC). For known chemical compositions, a Collison-type atomizer generated
90 singular-component solutions of ammonium sulfate, ((NH₄)₂SO₄, Acros 99.5%), sodium chloride, (NaCl, Acros
91 99+%) and succinic acid (C₄H₆O₄, Acros 99%) and subsequent internal mixture combinations as described in the
92 sections Aerosol Mixing States and Modified Mixing States: External to Internal. Succinic acid, classified as a slightly
93 soluble dicarboxylic acid, (18) (NH₄)₂SO₄, and NaCl are all relevant model atmospheric compounds with varying
94 degrees of solubility and hygroscopicity. All atomized solutions were prepared using Millipore[®] DI water (18 mΩ,
95 TOC ≤ 5 ppb). Atomized wet droplets were dried with silica gel diffusion dryer (as commonly practiced). In addition,
96 we employ a heated column before the diffusion dryer to facilitate the evaporation of water from the wet particles.
97 The implications of the use or absence of a heated column are discussed in the results below.

98 An AVL Particle Generator (APG), which houses a mini Combustion Aerosol STandard soot generator
99 (miniCAST 6203C, Jing ltd.), was used to generate carbonaceous aerosols. The APG consists of a propane burner
100 followed by a volatile particle remover. The burner was operated at 400°C with a propane and air flow rate of 15 ml
101 per min and 1.0 l per min, respectively. The aerosol structures generated by the APG likely consisted of fractal-like
102 agglomerates of non-spherical particles (Durdina et al., 2016). APG Combustion aerosols are mixed with inorganic
103 and slightly soluble succinic acid and CCN is subsequently measured at different supersaturations.



104 2.2 Aerosol Mixing Methods

105 Mixing compounds in solution can readily form internal mixtures of aerosol. (Gibson et al., 2007; Hameri et al.,
106 2002) Internal solutions of a highly hygroscopic compound, NaCl, and a slightly hygroscopic compound, succinic
107 acid, are shown. Five aqueous solutions of succinic acid and NaCl with molar ratios of 100:0, 87:13, 69:31, 43:57,
108 0:100 were aerosolized using a single atomizer, passed through a heated column, dried, and sampled directly into a
109 Scanning Mobility Particle Sizer (SMPS) and CCN Counter (CCNC).

110 External mixtures were formed via two methods. The first and simplest method required two sufficiently dry
111 aerosol streams to mix. Two aerosol streams were joined via a Swagelok® Tee connector. External mixtures were
112 also formed in a flow tube mixing apparatus. As conditions (e.g., but not limited to, residence time, temperature,
113 pressure, relative humidity) change in a flow tube, it is assumed that the external mixture may transition into an
114 internally mixed aerosol system. A flow tube mixing apparatus was constructed to test this assumption and modify
115 the extent of mixing of multiple components (Fig. 1 & 2).

116

117

118 **Figure 1.** External and Internal Mixtures with gradual mixing in flow tube

119

120 This work discusses changes in CCN experimental data and analysis as a result of changes in the extent of
121 mixing. Results of the CCN activation are presented in the Section: Modified Mixing: External to Internal Mixing in
122 the Aerosol Flow Tube. A brief description of the flow tube is provided here. The first aerosol stream is introduced
123 into the flow tube by a ¼ inch stainless steel (SS) tube. The second aerosol stream is also introduced by a ¼ inch SS
124 tube, but is expanded to an outer concentric ¾ inch SS tube using a SS Swagelok tee connection. The two aerosol
125 flows are initially mixed together at the exit of ¼ inch tube and aerosol mixes within the ¾ inch SS tube for an
126 additional 12 inches before entering the quartz tube where it continues to mix. In this study, the pressure and
127 temperature of the flow tube is maintained at ambient conditions. The extent of mixing in the flow tube mixer has
128 been modeled by Computational Fluid Dynamics simulation (CFD - Comsol) to test and improve the aerosol mixing
129 capabilities of the flow tube mixer (Fig. A1). The focus of this work is not the mixing apparatus but the CCN behavior



130 that results from changes in the extent of mixing. It is noted that particle losses likely occur within the flow tube
131 system but do not affect the intrinsic aerosol and CCN properties (activated fractions) presented here.

132

133 **Figure 2.** Example of charge corrected a) a single component activation curve b) a multiple activation curve from an
134 externally mixed/heterogeneous system. The asymptote, η , varies in height and length with the presence of mixed
135 components and their respective hygroscopicities.

136 2.3 CCN Activity and Chemical Composition: Measurements and Instrumentation

137 CCN activation is measured with particle sizing and counting instrumentation in parallel with CCN counting
138 instrumentation. This technique is widespread and has been used in numerous publications (Moore et al., 2010; Padró
139 et al., 2012). The development of a single continuous-flow thermal gradient diffusion column CCN Counter, CCNC
140 (Droplet Measurement Technologies, Inc.) has provided rapid (~ 1 Hz) and robust CCN data (Lance et al., 2012;
141 Roberts and Nenes, 2005). Aerosols with a S_c lower than the supersaturation in the column activate and form droplets.
142 These droplets are detected and counted using an optical particle counter at the exit of the column.

143 A TSI 3080 Electrostatic Classifier selects and measures aerosol size distributions. Polydisperse aerosol streams
144 are passed through a bi-polar krypton-85 charger and then through a differential mobility analyzer (DMA), where the
145 aerosols are sized according to electrical mobility with a sheath to aerosol flow ratio of 10:1. The monodispersed flow
146 is then split to a CPC and a CCN counter. CN concentrations were measured with a condensation particle counter,
147 CPC (TSI 3772, TSI 3776).

148 The CCNC is operated at 0.5 lpm with a sheath to aerosol flow ratio of 10:1 and is calibrated with $(\text{NH}_4)_2\text{SO}_4$ to
149 determine the instrument supersaturation (Rose et al., 2008). Operating the CCN in parallel with the CPC allows for
150 the simultaneous measurements of the total CN and CCN of the monodispersed aerosols. By operating the DMA in
151 scanning voltage mode and maintaining a constant column supersaturation, the CCN/CN, or activation ratio, as a
152 function of dry diameter can be obtained for a given supersaturation. These size resolved CCN distributions obtained
153 through scanning mobility CCN analysis (SMCA) are produce CCN activation curves, CCN/CN ratio as a function of
154 particle mobility diameter (Moore et al., 2010). SMCA produces high resolution CCN activation data near the 50%
155 efficiency critical diameter every ~ 2 minutes.



156 An Aerodyne high-resolution time-of-flight aerosol mass spectrometer (HR-ToF-AMS) measured the non-
157 refractory bulk composition (DeCarlo et al., 2006). The HR-ToF-AMS was operated in V-mode to track the
158 concentration and vacuum aerodynamic diameter as the aerosol fractions were modified.

159

160 3. CCN Analytical Method

161 CCN data analysis of single component aerosols, such as AS, are well characterized. The activation of a single
162 known component yields a simple sigmoidal activation curve and is often used for instrument calibration (Fig. 2a).
163 However ambient aerosols generally exist as complex mixtures of organic and inorganic species. CCN data sets from
164 ambient and chamber studies, which consist of these aerosol mixtures, may not show a single sigmoidal activation
165 curve but instead can exhibit multiple activation curves not associated with doubly charged particles (Fig. 2b).

166

167 Sigmoidal fits are applied to the CCN/CN as a function of dry activation diameters for the multicomponent
168 aerosols. Externally mixed aerosol fractions in activation curves have been previously observed in ambient studies by
169 Lance et al. (2013), Moore et al. (2012), and Bougiatioti et al. (2011). For those studies, E was defined as the
170 hygroscopic fraction, and $I-E$ the non-hygroscopic mixed fraction. For this study the first curve is similarly defined
171 as the hygroscopic externally mixed fraction (EMF) with an asymptote, or plateau of η . The dependence of η varies
172 with the presence of mixed components and their respective hygroscopicities. Thus we evaluate η for controlled
173 compositions and compare how representative they are of the known fractions of mixtures.

174 A sigmoidal fit through the EMF determines the particle dry diameter of the more hygroscopic species. A
175 second sigmoidal fit is applied to the second activation curve. An example is shown in Fig. 2b for an external
176 mixture of AS and SA. A sigmoid is fit for the more hygroscopic species, AS, and then a second for the less
177 hygroscopic species, SA. The activation diameters are consistent with those expected for the two compounds and
178 agree with Köhler predicted activation values for AS and SA. Doubly charge aerosols are indicated in Figure 2 and
179 are a negligible contribution to the activation curves.

180 The supersaturation and critical dry diameter are related via with the single parameter hygroscopicity, κ , to
181 describe the CCN activity and to determine the effect of mixing states of multiple components on the supersaturated



182 hygroscopic properties of aerosols. Using the generalized κ -Köhler equations presented by Petters and Kreidenweis
 183 (2007 and 2008), droplet growth in the supersaturated regimes for a selected dry diameter can be modeled for an
 184 aerosol where the entire particle diameter dissolves at activation.

$$185 \quad \ln S_c = \left(\frac{4A^3 \rho_w M_s}{27 v \rho_s M_w D_d^3} \right)^{1/2}, \quad \text{where } A = \frac{4\sigma_{s/a} M_w}{RT \rho_w} \quad (1)$$

$$186 \quad \kappa = \frac{4A^3}{27 D_d^3 \ln^2 S_c} \quad (2)$$

187 $\sigma_{s/a}$ is the surface tension, M_w is the molecular weight of water, R the universal gas constant, T is the temperature at
 188 activation, and ρ_w is the density of water. Surface tension and density of water were calculated according to
 189 temperature dependent parameterizations presented by Seinfeld and Pandis (1998) and Pruppacher and Klett (1997).
 190 The surface tension of the solution is assumed to be that of pure water. Traditional Köhler theory is known to work
 191 reasonably well for inorganic salts and slightly-soluble and hygroscopic organics like succinic acid.

192

193 4. Results and Discussion

194 4.1 Internal Mixtures

195 Aerosolized internally mixed solutions exhibit single CCN activation curves for all five compositions of
 196 succinic acid and NaCl solutions (Fig. 3a). The activation curve is similar to that of ammonium sulfate in Figure 2a.
 197 Multiply charged particles contribute less than 10% to the activated fraction and are assumed to be negligible. One
 198 sigmoid that plateaus near one can be applied to describe the CCN activation. As the internal mixture salt fraction
 199 increased at a given supersaturation, the single curve was maintained and shifted towards a lower activation diameter,
 200 indicative of and consistent with more hygroscopic aerosol. Using the simple mixing rule, a multicomponent
 201 hygroscopicity parameter can be theoretically derived based on the expected kappa values for each individual
 202 component hygroscopicity (κ_i), and the volume fraction of each component (ε_i) (Petters and Kreidenweis (2007)).

$$203 \quad \kappa = \sum_i \varepsilon_i \kappa_i \quad (3)$$



204 Equation (3) was applied for each mixture. κ was calculated and compared to the experimental values (Fig. 3b). These
205 internal mixtures do not strongly follow the simple mixing rule for every mixture and is consistent with the previous
206 work of Shulman et al. (1996) and Padró et al. (2007) who showed that slightly soluble compounds internally mixed
207 with salts resulted in surface tension depression and thus a lower required critical supersaturation. As previously
208 published, accounting for organic surface tension depression could improve kappa-hygroscopicity calculations for
209 internal mixtures. Regardless of prediction, the single sigmoidal experimental data set is indicative of a single
210 component or homogeneous internally mixed aerosol population.

211

212

213 **Figure 3. a)** Activation curves for two component internal mixtures of NaCl and succinic acid (SA) at SS 0.72%.

214 Doubly charged aerosols are present but are all below 0.1 and negligible. **b)** Internally mixed aerosols.

215 Multicomponent hygroscopicity parameter predictions vs. experimentally derived kappa values. Dashed lines

216 indicate 20% uncertainty.

217 4.2 External to Internal Aerosol Mixing Results

218 Individual single component aqueous solutions of ammonium sulfate (AS), $(\text{NH}_4)_2\text{SO}_4$, and succinic acid
219 (SA) were aerosolized, dried with an active heated column and silica gel diffusion dryer to produce external mixtures.
220 Data sets yielding multiple activation curves consistent with external mixing were successfully created by *i)* mixing
221 aerosol streams and *ii)* injecting SA and AS-compounds in the flow tube. For this manuscript, we show externally
222 mixed data generated from the use of the mixing flow tube. The direct mixing produces the same external mixed CCN
223 results (not shown). By using aerosols consisting of compounds of significantly different hygroscopicities, and thus
224 different activation diameters, distinct double plateaus for CCN activation can be observed for external mixtures (Fig.
225 2b). At particle mobility diameters between ~35 and 45 nm there is an asymptote, $\eta \sim 0.6$ (Fig. 4a., 4b., and 4c). The
226 activation curves were characteristic of AS and SA, and the measured activation diameters agreed well with Köhler
227 Theory and the single parameter (κ) thermodynamic predictions of droplet activation (Fig. 4a). The external mixture
228 was maintained for an hour as indicated by the separate and stable activation diameters derived from multiple sigmoid
229 analysis.



230

231

232 **Figure 4. External to internal mixtures of a slightly soluble organic aerosol, succinic acid (SA) and inorganic**
233 **ammonium sulfate (AS) aerosol.** The CCNC was operated at a single S_c of 0.8%. Closed symbols are externally
234 mixed. Open symbols are internally mixed. a) The apparent kappa values derived from externally mixed multiple-
235 sigmoid activation data before active heating is turned off at approximately 3:30 pm and after 3:30pm where single
236 sigmoid activation curves are observed. The two dotted lines indicate the theoretically derived kappa values for
237 succinic acid, $\kappa=0.23$, and ammonium sulfate, $\kappa=0.61$. b) CCN activation curves exhibit external (with active
238 heating before 3:30 pm) and then transitioning external to internal mixing (after 3:30pm) c) CCN/CN vs. Dry
239 mobility diameter data as a function of time. The asymptote, η , disappears at the by the end of the experiment.

240

241 After one hour in the flow tube, the active heating column was turned off. It should be noted that atomized
242 aerosol continued to be dried through the silica gel diffusion dryers, as is commonly done. The relative humidity after
243 the dryer in both cases is small ($< 20\%$) and thus the activation diameters of very hygroscopic AS calibration aerosol
244 are not affected with or without active heating (Fig. A2). However, as soon as active heating was turned off, particles
245 in the mixing flow tube became more mixed (Figure 4). Thus, it is likely that minute amounts of aerosol water
246 promoted internal mixing and shifted aerosol mixing from external to internal in the mixing flow tube system.

247 CCN activation curves for the two compounds remained distinct and separate until internal mixing conditions
248 dominated and the multiple CCN activation curves converged into a single curve (Fig. 4b and 4c). Results suggest
249 aerosol water plays a significant factor in mixing and CCN activation. This is consistent with previous work that
250 indicates that the presence of water led to lowered aerosol viscosity and increased diffusivity (Ye et al., 2016). The
251 wetted aerosols can come in contact through diffusion and coalesce to form an internally mixed aerosol. The apparent
252 kappa values from fitting the two individual activation curves for the external part of the mixing experiment and
253 subsequent internal mixing are shown in Fig. 4a.

254 To help track the change in organic/inorganic fractions during the transition from external to internal, the
255 mixed aerosols were analyzed with a high-resolution time of flight mass spectrometer (HR-ToF-AMS) to provide mass
256 fraction information. The mass size distribution was integrated and normalized for each compound per scan according
257 to the total mass that was measured. The mass size distribution was then converted to number size distribution and the



258 diameters were converted from aerodynamic diameter to electrical mobility diameter. Then for each superstation and
259 fraction, the EMF was calculated between the two respective activation diameters and correlated to the EMF that was
260 determined from SMCA to determine the plateau height (η).

261 AS fractions measured by the AMS are consistent with the changes SMCA derived η where increases in AS
262 mass fraction increase η . However, the AMS derived AS fraction are slightly lower compared to SMCA (Figure 5),
263 indicating potential influence on η from other factors. Previous work has shown the presence of highly soluble
264 materials (like AS) can promote CCN activity of organic dominated systems (Asa-Awuku et al., 2011; Fofie et al.,
265 2017). A second flow tube experiment was conducted to test the effect of differing concentrations on plateau heights.
266 The detection efficiency for particles with smaller sizes in the AMS (<50nm) can effect the AS fraction. Thus, the
267 CCNC supersaturation was modified from 0.2 to 1.2% to test the effect of activation diameter on closure (Fig. 6).
268 Results show good agreement and are within 20% of predictions. Results utilizing CCN activation data for aerosols
269 <50nm may be a good substitute for estimating aerosol chemical fractions when other instruments with lower size
270 resolution are not readily available.

271

272

273 **Figure 5.** Plateau heights derived from AMS data vs. SMCA. Single CCNC Supersaturation

274

275

276 **Figure 6.** Modifying activation diameters. Plateau heights derived from AMS data vs. SMCA for CCNC

277

Supersaturation from 0.2 to 1.2%

278

279

280 **4.3 External and Internal Mixtures of Combustion Aerosol**

281

282 Combustion Aerosol, hereon also referred to as Black Carbon (BC) can form external and internal complex
283 aerosol mixtures. BC is considered insoluble but wettable and the contributions of BC to aerosol-cloud interactions at
284 varied mixing states is not well known or understood. Thus the ability of BC to mix with inorganic and organic
285 compounds and observe the extent of mixing as they activate as CCN is of great interest.



286 Prior to investigating the impact of mixing fresh combustion emissions with inorganic and organic aerosols, the
287 CCN activation spectra of combustion was defined using combustion aerosol derived from the APG.

288 CCN activated fraction data from combustion aerosol was fit to a singular sigmoidal curve (Fig. 7). The
289 single sigmoid fit suggests that the aerosol generated is a homogenous mixture of black and brown carbon. Combustion
290 aerosol activated at a mobility diameter of 133 nm at 2.2% supersaturation. The apparent hygroscopicity of combustion
291 aerosol was $\kappa=0.001$, and is consistent with the order of magnitude and kappa values reported for fresh combustion
292 aerosol from diesel engine sources (Fig. 7) (Vu et al., 2015). It is noted that the apparent hygroscopicity does not
293 account for non-spherical fractal particles.

294

295

296 **Figure 7.** Combustion aerosol activation curve (SS 2.2%, $d_{p,50}=133\text{nm}$, $\kappa=0.001$)

297

298 Next, the influence of modifying externally mixed hygroscopic aerosol fractions with non-hygroscopic BC was
299 observed. BC was externally mixed with various concentrations of AS and NaCl in two separate experiments. For
300 each BC mixture, combustion aerosol was introduced to the flow tube and atomized inorganic and organic aerosol
301 (dried with a heated column and silica gel diffusion dryers) was injected. The concentration of inorganic in the flow
302 tube was slowly increased to modify the contribution of soluble material. The CCN counter supersaturation was
303 decreased to 1.1% to observe the impact of the more hygroscopic compounds in the BC mixture.

304

305 Figure 8 shows the CCN activation of external mixtures of BC with AS and NaCl at $S_c = 1.1\%$. The initial
306 combustion size distribution at the start of the experiment and the modified CCN activation fractions of the aerosol
307 mixtures are presented. The shape of the activation curve provides insight about the sizes of very hygroscopic and
308 non-hygroscopic species. At $S_c = 1.1\%$ BC particles, with $\kappa = 0.001$, will not theoretically activate below 250 nm and
309 the contribution of externally mixed BC in the size range shown does not contribute much (if any) CCN. The
310 normalized size distribution data show that there are few BC particles at small sizes ($<50\text{ nm}$), the majority of particles
311 in this range are inorganic. Thus for both the AS and NaCl external mixtures, the activation diameters derived from a
312 singular fit were consistent with the expected $dp_{50} < 50\text{ nm}$ of the respective inorganic salts. At the larger sizes ($>$
313 inorganic d_{p50}), the BC concentration increased and the CCN/CN was depressed. The combustion aerosol alone is not



314 CCN active at this S_c or size and the depressions are reflective of the non-hygroscopic combustion aerosol fraction in
315 the aerosol sample. Notably, plateaus are dynamic. As the concentration of inorganic salts increase, the increased
316 activated fraction is reflected in the CCN spectra; the plateau heights increase with increasing hygroscopic
317 concentrations. In these particular externally mixed experiments, the initial CCN/CN plateau can be as large as one,
318 subsequently decrease, and then will likely increase to one after the BC critical diameters are reached. BC externally
319 mixed with very hygroscopic material is observed to be more CCN active than BC alone.

320

321

322 **Figure 8.** Combustion aerosols externally mixed with inorganics a) NaCl externally mixed with concentrations
323 modified from 51% to 85% over the course of 60 min b) AS externally mixed with concentrations from 41% to 86%
324 over a course of 75 min. Cross symbols represent the initial size distribution of the combustion aerosol.

325

326 Succinic acid (SA) was mixed with combustion aerosol to investigate the external to internal mixing and transition of
327 slightly hygroscopic organic with non-hygroscopic insoluble but wettable aerosols. The laboratory system mimics
328 observed increases in SOA mass fractions on combustion aerosols during atmospheric aging. The SA was introduced
329 to the flow tube at various concentrations, followed by the combustion aerosol from the APG, under dry externally
330 mixed conditions and bimodal size distribution peaks were observed (Figure 9).

331

332

333 The normalized size distributions of the aerosol leaving the flow tube are presented. The initial BC size distribution
334 is similar to those presented in Figure 8. Assuming the first of the two peaks is SA, and the second is a mixture of the
335 combustion aerosol and SA, the initial point of activation agrees with that of succinic acid where SA aerosols all
336 activate. After a mobility diameter, $dp > 50$ nm, the concentration of combustion aerosol in the mixture increases
337 and the CCN/CN ratio is < 0.2 , indicative of a lower SA concentration relative to the non-activated BC concentration.

338

339 To induce internal mixing, active heating was again turned off for the atomized aerosol source. Again, internal mixing
340 was promoted and the multiple activation curves converge into a single sigmoid for the BC and SA system. This is
341 consistent with the AS/SA experiment and previous work that showed a strong influence of insoluble compounds on



342 activation when internally mixed with a more soluble compound. (9) With continued mixing, a shift to larger activation
343 diameters was observed towards the end of the experiment (scan 93) and there was a slight depression in the plateau
344 of the CCN spectra.

345

346 The data suggests that only a small amount of soluble inorganic and organic material is required to make the BC more
347 active than that observed alone, especially as the aerosol becomes more internally mixed.

348

349

350 **Figure 9.** a) Time series of CCN/CN activated fractions of Succinic Acid (SA) and combustion aerosol (BC)

351 mixture in flow tube. b) Succinic Acid and Combustion Aerosol mixtures for Scans 24, 45, 54, 73, and 94. Aerosol

352 water is introduced at ~ scan 70 to promote internal mixing.

353

354 5. Conclusion

355 Results show that the experimental CCN activation curves of aerosol provide insight into to the type of mixing
356 (e.g. internal vs. external) and the various levels of hygroscopicities that are chemically representative. Modifications
357 in the concentrations of externally mixed non-hygroscopic aerosols are reflective of the CCN activated concentrations.
358 This is consistent with CCN spectra observed in ambient studies, which have attributed increases in plateau height to
359 the extent of internal mixing of hygroscopic materials on externally mixed inactivated aerosols. This work adds to the
360 existing body of CCN literature and demonstrates that the transition from external to internal mixtures can be
361 mimicked in controlled laboratory experiments and observed in CCN data. If one accounts for multiple-sigmoid
362 analysis in experimental CCN activation data, the CCN behavior of known hygroscopic compound mixtures (e.g.,
363 ammonium sulfate, sodium chloride, succinic acid) agrees well with traditional Köhler theory. However, more work
364 is needed to explore mixtures of hygroscopic material with wettable and non-hygroscopic aerosol. Here, as the non-
365 hygroscopic combustion aerosol becomes coated or internally mixed with the inorganic and organic material, the CCN
366 activity of the combustion aerosol is modified. The data here, with recent publications (Altaf et al., 2018; Ye et al.,
367 2016), suggest that aerosol water is a significant factor in promoting mixing and can be used to modify mixing states.



368 The aerosols maintained an external mixture under dry conditions; CCN activation curves plateaued and remained
369 constant. However, turning off the heater promoted internal mixing and the activation curves were observed to
370 converge. These experiments with known compounds confirm that the aerosol mixing state can be observed in CCN
371 activation data and can thus be revisited in complex aerosol data sets to understand the extent of mixing. The results
372 confirm that CCN counters and CCN analysis can be used in future studies to quantify the extent of mixing of ambient
373 particles. The results are critical to understanding other factors important to the direct and indirect radiative
374 contributions of atmospheric particles.

375

376 Acknowledgments

377 This work was supported by the University of California Transportation Center and the U.S. Environmental
378 Protection Agency (EPA) grant number 83504001. Diep Vu thanks the U.S. Environmental Protection Agency (EPA)
379 STAR Fellowship Assistance Agreement no. FP-91751101. EPA 83504001 was fundamental for the development of
380 the mixing flow tube apparatus. Additionally, AA would like to thank the National Science Foundation (NSF) proposal
381 1151893. The contents of this paper are solely the responsibility of the grantee and do not necessarily represent the
382 official views of the EPA or NSF. Further, the EPA and NSF do not endorse the purchase of any commercial products
383 or services mentioned in the publication. In addition the authors would like to acknowledge Desiree Smith, Drs. Kent
384 Johnson and Heejung Jung for their role in the acquisition of APG and access to controlled BC measurement and
385 Dr Jeffrey Pierce for advice on CCN models.

386

387 Appendix

388

389 **Figure A1.** Fluid dynamics simulation results of the flow stream transporting behaviors in the flow tube mixer

390



391 **Figure A2.** Atomized AS CCN calibrations. In both cases the aerosol is atomized and passed through a silica gel
392 diffusion dryer. The aerosol passes through a heated column before the drier in Dp_Heater on data and does no in
393 Dp_Heater off. The critical activation mobility diameters (μm) for heated-dried vs. non-heated dried atomized
394 sample streams agree. The two-tailed P-value is 0.87.

395

396

397 **References**

398

- 399 1. Abbatt, J. P. D., Broekhuizen, K., and Kumar, P. P.: Cloud condensation nucleus activity of internally mixed
400 ammonium sulfate/organic acid aerosol particles, *Atmos. Environ.*, 39, 4767-4778, 2005.
- 401 2. Altaf, M. B. Dutcher, D D. Raymond, T. M and Freedman, M. A.: Effect of Particle Morphology on Cloud
402 Condensation Nuclei Activity, *ACS Earth and Space Chem.*, 10.1021/acsearthspacechem.7b00146. 2018.
- 403 3. Asa-Awuku, A., Moore, R., Nenes, A., Bahreini, R., Brock, C. A., Middlebrook, A., Holloway, J., Ryerson, T.,
404 Jimenez, J., DeCarlo, P., Hecobian, A., Weber, R., Tanner, D., Stickel, R., and Huey L. G., 'Airborne Cloud
405 Condensation Nuclei Measurements during the 2006 Texas Air Quality Study, *J. Geophys. Res.*, 116,
406 doi:10.1029/2010JD014874. 2011.
- 407 4. Bhattu, D., Tripathi, S. N., and Chakraborty, A.: Deriving aerosol hygroscopic mixing state from size-resolved
408 CCN activity and HR-ToF-AMS measurements, *Atmos. Environ.*, 142, 57-70, 2016.
- 409 5. Bilde, M. and Svenningsson, B.: CCN activation of slightly soluble organics: The importance of small amounts
410 of inorganic salt and particle phase, *Tellus*, 56B, 128–134, 2004.
- 411 6. Bougiatioti, A., Nenes, A., Fountoukis, C., Kalivitis, N., Pandis, S. N., and Mihalopoulos, N.: Size-resolved CCN
412 distributions and activation kinetics of aged continental and marine aerosol, *Atmos. Chem. Phys.*, 11, 8791-8808,
413 doi:10.5194/acp-11-8791-2011, 2011.
- 414 7. Broekhuizen, K., Kumar, P. P., and Abbatt, J. P. D.: Partially soluble organics as cloud condensation nuclei: Role
415 of trace soluble and surface active species, *Geophys. Res. Lett.*, 31, doi:10.1029/2003GL018203, 2004.



- 416 8. Cruz, C. N. and Pandis, S. N.: The effect of organic coatings on the cloud condensation nuclei activation of
417 inorganic atmospheric aerosol, *J. Geophys. Res.*, 103, 13111-13123, 1998.
- 418 9. DeCarlo, P. F., Kimmel, J. R., Trimborn, A., H., Northway, M. J., Jayne, J. T., Aiken, A. C., Gonin, M., Fuhrer,
419 K., Horvath II, T., Docherty, K. S., Worsnop, D. R., Jimenez, J. L.: Field Deployable, High-Resolution, Time-of-
420 Flight Aerosol Mass Spectrometer, *Anal. Chem.*, 78, 8281-8289, 2006.
- 421 10. Durdina, L., Lobo, P., Trueblood, M.B., Black, E.A., Achterberg, S., Hagen, D., Brem, B.T., and Wang, J.:
422 Response of black carbon-mass instruments to mini-cast soot, *Aerosol Sci. Technol.*, 50, 906-918, 2016.
- 423 11. Dusek, U., Frank, G. P., Hildebrandt, L., Curtius, J., Schneider, J., Walter, S., Chand, D., Drewnick, F., Hings,
424 S., Jung, D., Borrmann, S., and Andreae, M. O.: Size matters more than chemistry for cloud-nucleating ability of
425 aerosol particles, *Science*, 312, 1375–1378, 2006.
- 426 12. Ervens, B., Cubison, M., Andrews, E., Feingold, G., Ogren, J. A., Jimenez, J. L., DeCarlo, P., and Nenes, A.:
427 Prediction of cloud condensation nucleus number concentration using measurements of aerosol size distributions
428 and composition and light scattering enhancement due to humidity, *J. Geophys. Res.*, 112,
429 doi:10.1029/2006JD007426, 2007.
- 430 13. Fofie, E. A., N. M. Donahue, and Asa-Awuku, A.: Cloud condensation nuclei activity and droplet formation of
431 primary and secondary organic aerosol mixtures, *Aerosol Sci. Technol.*, 52, 1-10, 2017.
- 432 14. Gibson, E. R., Gierlus, K. M., Hudson, P. K., and Grassian, V. H.: Generation of Internally Mixed Insoluble and
433 Soluble Aerosol Particles to Investigate the Impact of Atmospheric Aging and Heterogeneous Processing on the
434 CCN Activity of Mineral Dust Aerosol, *Aerosol Sci. Technol.*, 41, 914-924, doi: 10.1080/02786820701557222,
435 2007.
- 436 15. Hameri, K., Charlson, R. and Hansson, H. C.: Hygroscopic Properties of Mixed Ammonium Sulfate and
437 Carboxylic Acids Particles, *AIChE J.*, 48, 1309–1316, 2002.
- 438 16. Henning, S., Rosenørn, T., D'Anna, B., Gola, A. A., Svenningsson, B., and Bilde, M.: Cloud droplet activation
439 and surface tension of mixtures of slightly soluble organics and inorganic salt, *Atmos. Chem. Phys.*, 5, 575-582,
440 doi:10.5194/acp-5-575-2005, 2005.
- 441 17. Lance, S., Raatikainen, T., Onasch, T., Worsnop, D. R., Yu, X.Y., Alexander, M. L., Stolzenburg, M. R.,
442 McMurry, P. H., Smith, J. N., and Nenes, A.: Aerosol mixing-state, hygroscopic growth and cloud activation



- 443 efficiency during MIRAGE 2006, *Atmos. Chem. Phys. Discuss.*, 12, 15709–15742, doi:10.5194/acpd-12-15709-
444 2012, 2012.
- 445 18. Lance, S., Onasch, T., Warsnop, D., Yu, X. Y., Alexander, L., Stolzenberg, M., McMurry, P., Smith, J.N., Nenes.,
446 A.: Aerosol Mixing-State and Cloud Activation Efficiency during the MILAGRO Campaign, 2013, *Atmos.*
447 *Chem. Phys.*, 13, 5049-5062, doi:10.5194/acp-13-5049-2013, 2013.
- 448 19. Liu, D., Allan, J., Whitehead, J., Young, D., Flynn, M., Coe, H., McFiggans, G., Fleming, Z. L., and Bandy, B.:
449 Ambient black carbon particle hygroscopic properties controlled by mixing state and composition, *Atmos. Chem.*
450 *Phys.*, 13, 2015-2029, doi:10.5194/acp-13-2015-2013, 2013.
- 451 20. Moore, R. H., Nenes., A. and Medina., J.: Scanning Mobility CCN Analysis - A Method for Fast Measurements
452 of Size-Resolved CCN Distributions and Activation Kinetics, *Aerosol Sci. Technol.*, 44, 861-871, 2010.
- 453 21. Moore, R. H., Cerully, K., Bahreini, R., Brock, C. A., Middlebrook, A. M. and Nenes, A.: Hygroscopicity and
454 composition of California CCN during summer 2010, *J. Geophys. Res.*, 117, D00V12,
455 doi:10.1029/2011JD017352, 2012.
- 456 22. Padró, L. T., Asa-Awuku, A., Morrison, R., and Nenes, A.: Inferring thermodynamic properties from CCN
457 activation experiments: single-component and binary aerosols, *Atmos. Chem. Phys.*, 7, 5263-5274,
458 doi:10.5194/acp-7-5263-2007, 2007.
- 459 23. Padró, L. T., Moore, R. H., Zhang, X., Rastogi, N., Weber, R. J., and Nenes, A.: Mixing state and compositional
460 effects on CCN activity and droplet growth kinetics of size-resolved CCN in an urban environment, *Atmos. Chem.*
461 *Phys.*, 12, 10239-10255, doi:10.5194/acp-12-10239-2012, 2012.
- 462 24. Petters, M. D. and Kreidenweis, S. M.: A single parameter representation of hygroscopic growth and cloud
463 condensation nucleus activity – Part 2: Including solubility, *Atmos. Chem. Phys.*, 8, 6273-6279, doi:10.5194/acp-
464 8-6273-2008, 2008.
- 465 25. Petters, M. D. and Kreidenweis, S. M.: A single parameter representation of hygroscopic growth and cloud
466 condensation nucleus activity, *Atmos. Chem. Phys.*, 7, 1961-1971, doi:10.5194/acp-7-1961-2007, 2007.
- 467 26. Pruppacher, H. R. and Klett, J. D.: *Microphysics of Clouds and Precipitation*, 954, Kluwar Acad., Norwell Mass.,
468 1997.
- 469 27. Roberts, G. C. and Nenes, A.: A Continuous-Flow Streamwise Thermal-Gradient CCN Chamber for Atmospheric
470 Measurements, *Aerosol Sci. Technol.*, 35, 206-2011, doi: 10.1080/027868290913988, 2005.



- 471 28. Rose, D., Gunthe, S. S., Mikhailov, E., Frank, G. P., Dusek, U., Andreae, M. O., Pöschl, U.: Calibration and
472 measurement uncertainties of a continuous-flow cloud condensation nuclei counter (DMT-CCNC): CCN
473 Activation of ammonium sulfate and sodium chloride aerosol particles in theory and experiment, *Atmos. Chem.*
474 *Phys.*, 8, 1153-1179, doi: 10.5194/acp-8-1153-2008, 2008.
- 475 29. Saxena, P., Hildemann, L. M.: Water-Soluble organics in atmospheric particles: A critical review of the
476 literature and application of thermodynamics to identify candidate compounds, *J. Atmos. Chem.*, 24, 57-109,
477 1996.
- 478 30. Seinfeld, J. H. and Pandis, S. N.: *Atmospheric Chemistry and Physics*, John Wiley, New York, 1998.
- 479 31. Shulman, M. L., Jacobson, M. C., Charlson, R. J., Synovec, R. E., and Young, T. E.: Dissolution behavior and
480 surface tension effects of organic compounds in nucleating cloud droplets, *Geophys. Res. Lett.*, 23, 277-280,
481 1996.
- 482 32. Sullivan R. C., Moore M., Petters, M. D., Kreidenweis S. M., Roberts G. C., and Prather, K. A.: Effect of chemical
483 mixing state on the hygroscopicity and cloud nucleating properties of calcium mineral dust particles, *Atmos.*
484 *Chem. Phys.*, 9, 3303-3316, 2009.
- 485 33. Svenningsson, B., Rissler, J., Swietlicki, E., Mircea, M., Bilde, M., Facchini, M. C., Decesari, S., Fuzzi, S., Zhou,
486 J., Mønster, J., and Rosenørn, T.: Hygroscopic growth and critical supersaturations for mixed aerosol particles of
487 inorganic and organic compounds of atmospheric relevance, *Atmos. Chem. Phys.*, 6, 1937-1952,
488 doi:10.5194/acp-6-1937-2006, 2006.
- 489 34. Vu, D., Short, D., Karavalakis, G., Durbin, T. D., and Asa-Awuku, A.: Integrating cloud condensation nuclei
490 predictions with fast time resolved aerosol instrumentation to determine the hygroscopic properties of emissions
491 over transient drive cycles, *Aerosol Sci. Technol.*, 49, 1149-1159, 2015.
- 492 35. Wex, H., McFiggans, G., Henning, S., and Stratmann, F.: Influence of the external mixing state of atmospheric
493 aerosol on derived CCN number concentrations, *Geophys. Res. Lett.*, 37, doi:10.1029/2010GL043337, 2010.
- 494 36. Ye, Q., Robinson, E. S., Ding, X., Ye, P., Sullivan, R., and Robinson, N.: Mixing of secondary organic aerosols
495 versus relative humidity, *Proc. Natl. Acad. Sci. U. S. A.*, 113, 12649-12654, 2016.

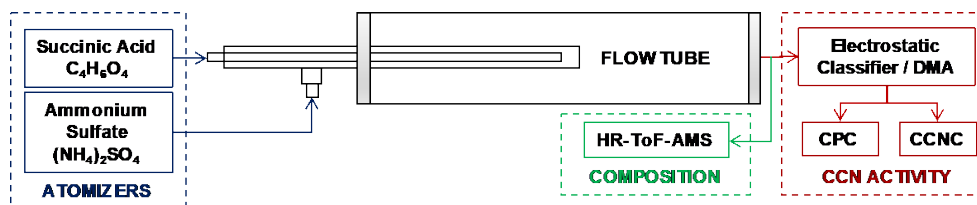


fig01

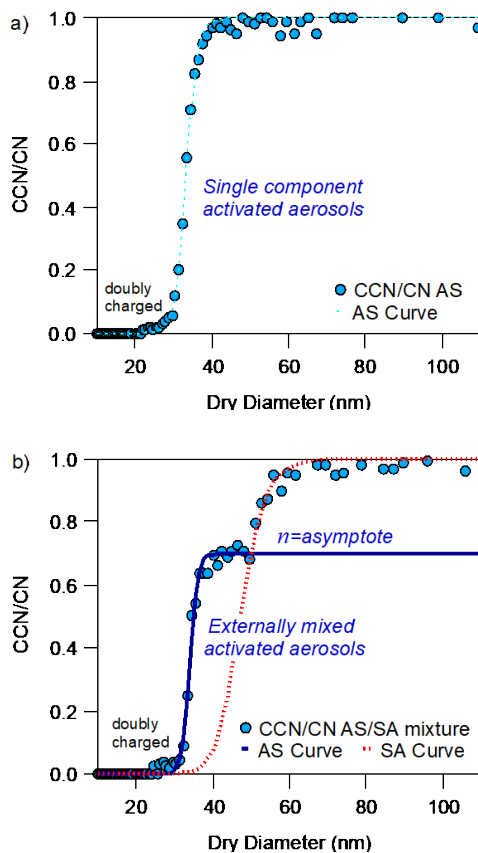


fig02

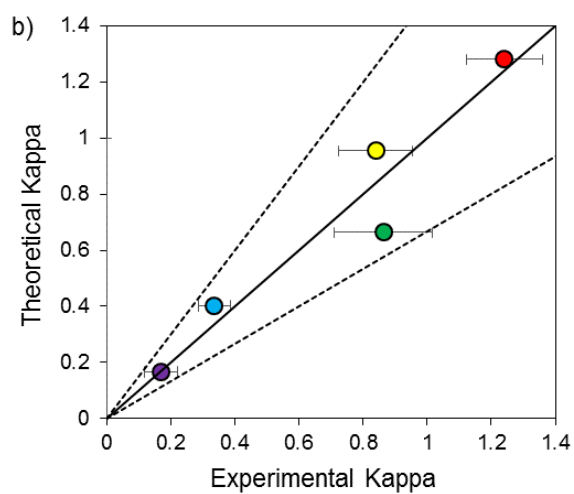
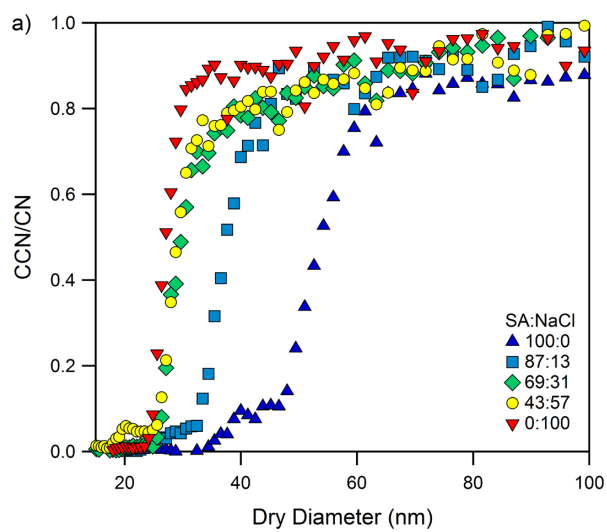
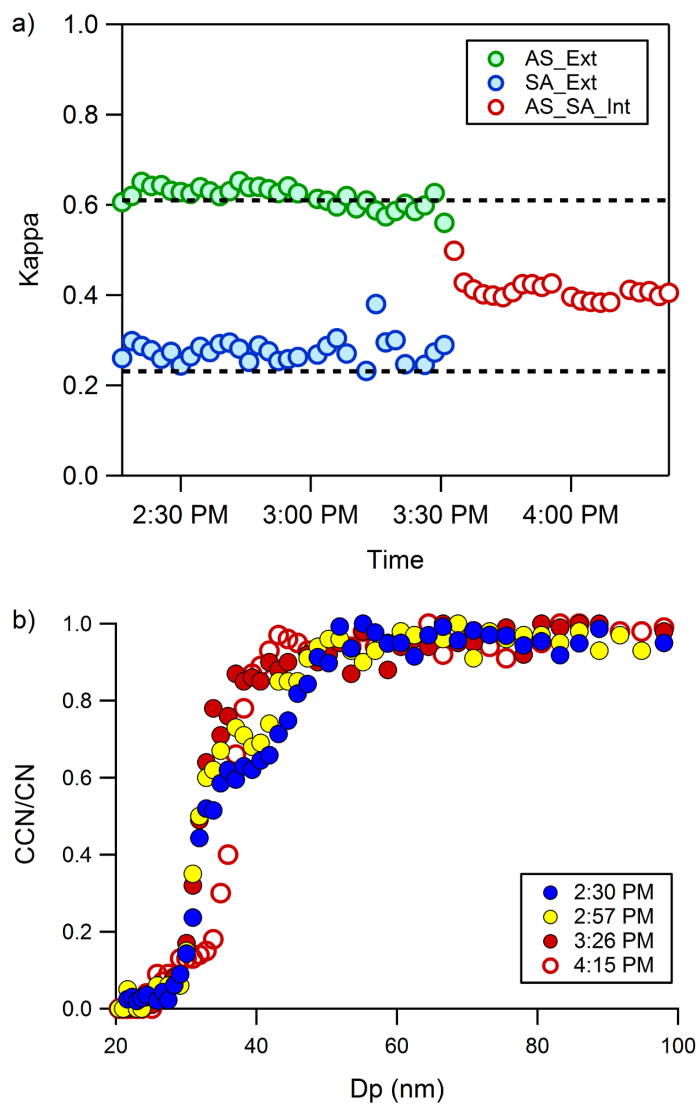


fig03



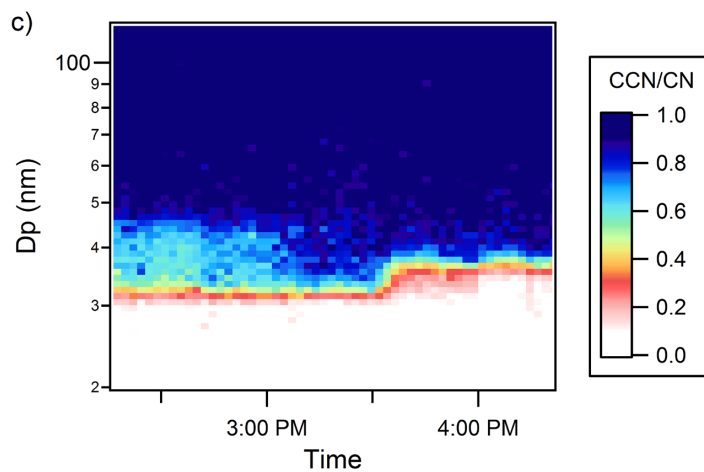


fig04

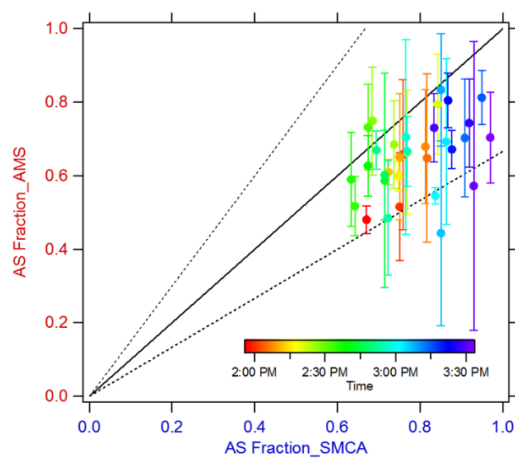


Fig05

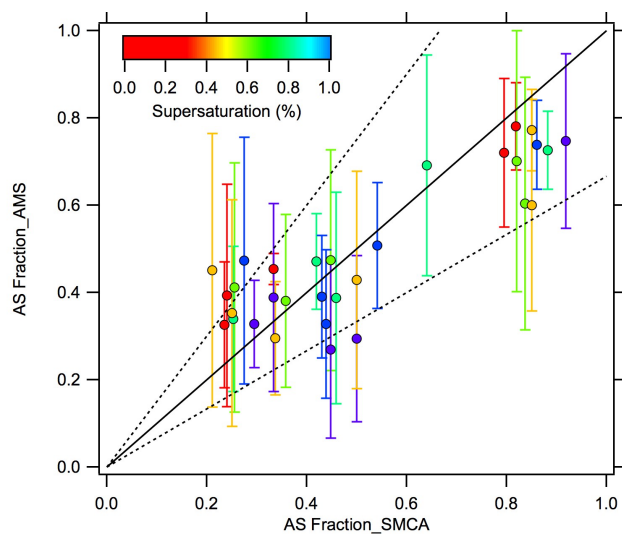


fig06

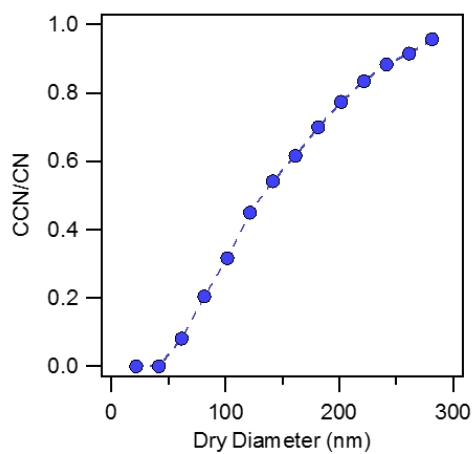


fig07

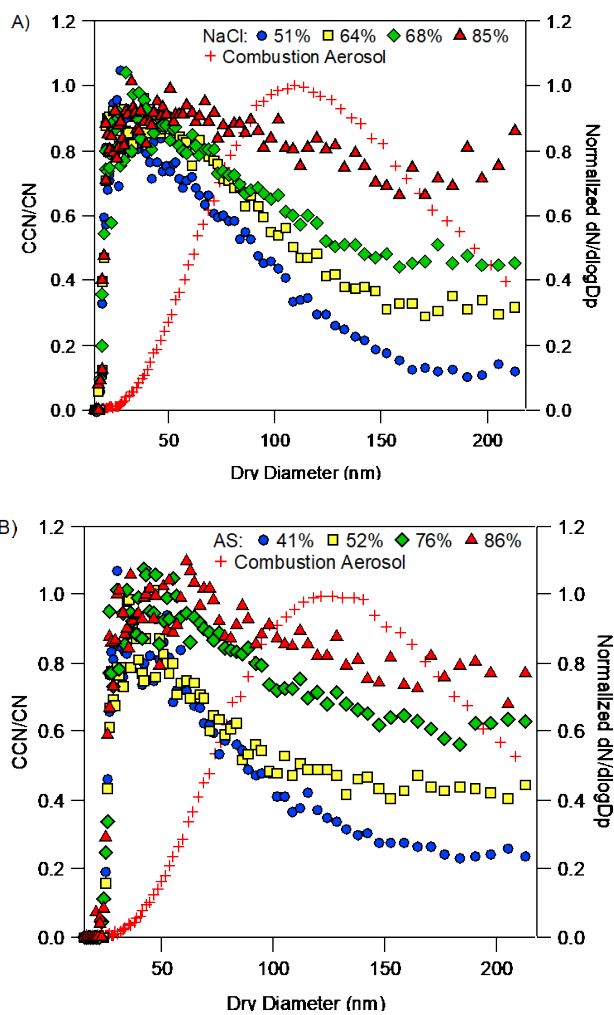
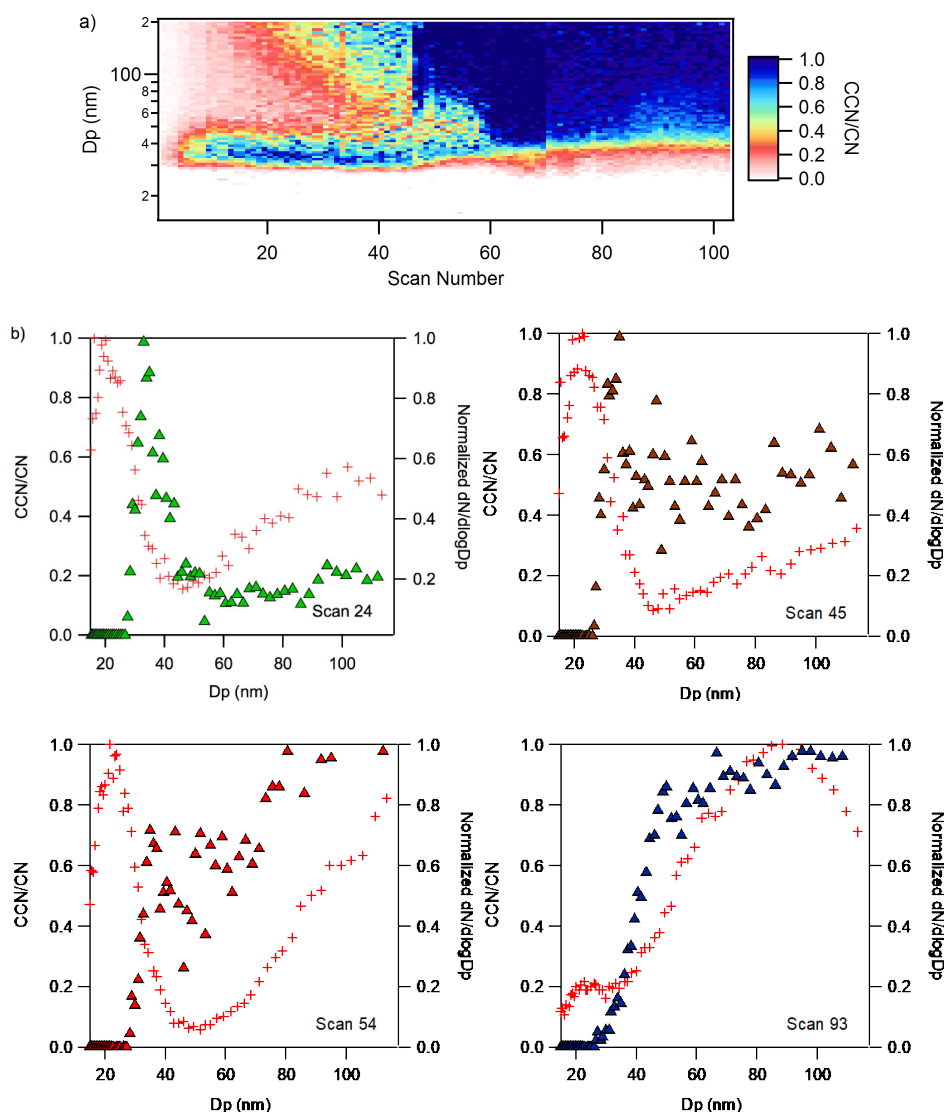


fig08



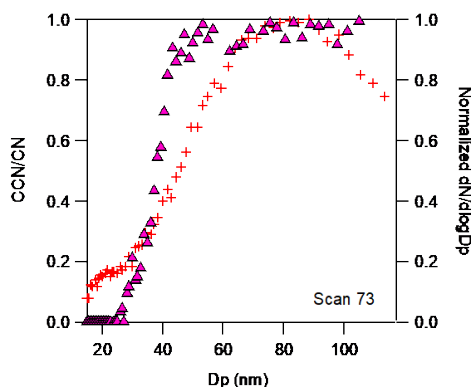


Fig09

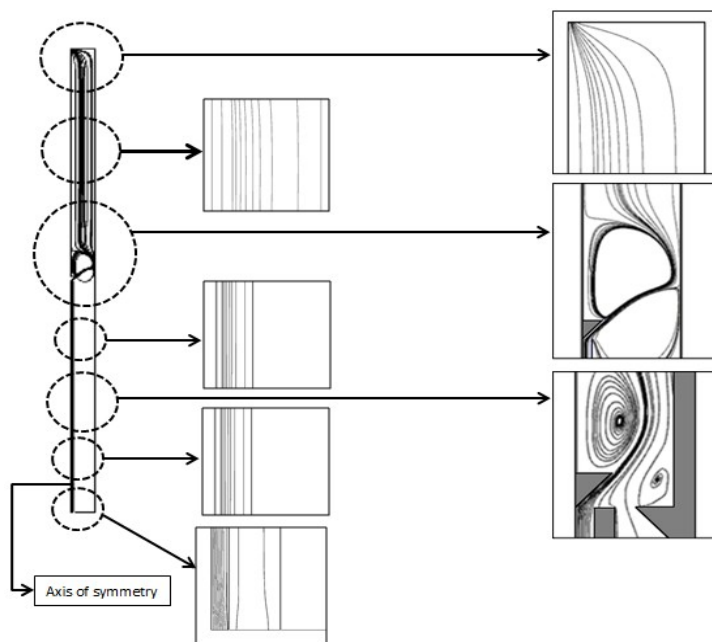


Fig0A1

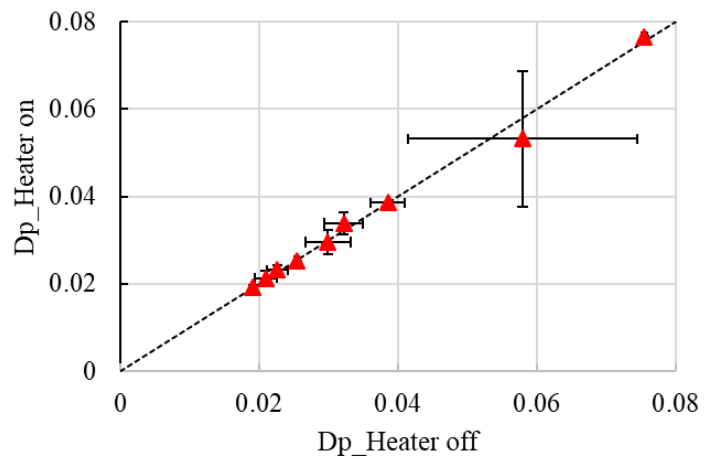


Fig0A2